

# Simultaneous Destriping and Denoising for Remote Sensing Images With Unidirectional Total Variation and Sparse Representation

Yi Chang, Luxin Yan, Houzhang Fang, and Hai Liu

**Abstract**—Remote sensing images destriping and denoising are both classical problems, which have attracted major research efforts separately. This letter shows that the two problems can be successfully solved together within a unified variational framework. To do this, we proposed a joint destriping and denoising method by integrating the unidirectional total variation and sparse representation regularizations. Experimental results on simulated and real data in terms of qualitative and quantitative assessments show significant improvements over conventional methods.

**Index Terms**—Denoising, destriping, remote sensing image, sparse representation, unidirectional total variation (UTV).

## I. INTRODUCTION

REMOTE sensing images often suffer from stripe noise and random noise, which greatly degrade the image quality and limit the applications [1], [2]. In multidetector imaging systems, stripe noise is mainly caused by the different responses of each detector, whereas random noise arises from photon effects and electronic noise. In the past decades, destriping and denoising tasks have attracted major research efforts and been treated separately. Destriping approaches can be roughly categorized into three groups, i.e., digital filtering-based methods [3], [4], statistical matching-based methods [5], [6], and variational model-based methods [7]–[9]. Some denoising methods such as total variation (TV) [10] and wavelets [11]–[13] have been developed for remote sensing images.

In reality, however, stripes and random noise coexist in remote sensing images. Conventionally, a natural solution would be to first perform a denoising process and then feed the denoised result into a destriping process and vice versa. In [3], the authors proposed first applying the wavelet Fourier adaptive filter (WFAF) to destripe, followed by wavelet-based denoising algorithm to suppress noise. However, if the destriping process is accomplished first, the existing random noise may increase the difficulty in removing the stripes, resulting in the residual stripes in the result. On the contrary, if the denoising process

is performed first, the regular pattern of stripes would be unavoidably damaged, making the next destriping process more challenging. As far as we know, few works have been done to simultaneously remove stripe noise and random noise.

It is noteworthy that both destriping and denoising tasks have been modeled as inverse problems and tackled by regularization successfully. It motivates us to develop a unified variational framework to simultaneously destripe and denoise in remote sensing images. In this letter, the key idea is to construct regularizations combining the unidirectional TV (UTV) and sparse representation over learned dictionary (SLD) to constrain the solution. The UTV helps remove stripes, whereas the SLD is beneficial for suppressing random noise. The split Bregman iteration is adopted to solve the resulting minimization problem. Our method has been validated by experiments on Moderate Resolution Imaging Spectroradiometer (MODIS) images and Hyperion onboard Earth Observation-1 (EO-1) satellite images.

## II. PROBLEM FORMULATION

### A. Degradation Model

Assuming stripe noise and random noise are additive [8]–[10], the degradation process due to stripes and random noise can be described as

$$\mathbf{f} = \mathbf{u} + \mathbf{n} \quad (1)$$

where  $\mathbf{f}$  denotes the striped and noisy image, and  $\mathbf{u}$  is the latent clear image. Note that, in this letter, the noise  $\mathbf{n}$  includes both stripe noise and random noise. Formally, our task is to estimate the latent clear image  $\mathbf{u}$  with the given image  $\mathbf{f}$  in the presence of both stripes and random noise  $\mathbf{n}$ . It is a typical ill-posed inverse problem. The key is to construct appropriate regularization terms to suppress both stripes and random noise at the same time.

### B. UTV for Destriping

TV is very popular for destriping because of the property of edge preserving [10]. Shen and Zhang [7] first proposed a maximum *a posteriori*-based destriping method with a Huber–Markov prior, which is an alternative between the isotropic TV and Tikhonov regularization. A similar prior was also utilized in [8]. Specially, stripes have clear directional signature. Therefore, an anisotropic TV is preferred over the isotropic ones for the destriping task [9]. To illustrate, in

Manuscript received August 27, 2013; accepted September 30, 2013. This work was supported in part by the Fundamental Research Funds for the Central Universities, Huazhong University of Science and Technology, under Grant 2013TS131 and in part by the National Natural Science Foundation of China under Grant 60902060.

The authors are with the Key Laboratory of Ministry of Education for Image Processing and Intelligent Control, School of Automation, Huazhong University of Science and Technology, Wuhan 430074, China (e-mail: yanluxin@gmail.com).

Color versions of one or more of the figures in this paper are available online at <http://ieeexplore.ieee.org>.

Digital Object Identifier 10.1109/LGRS.2013.2285124

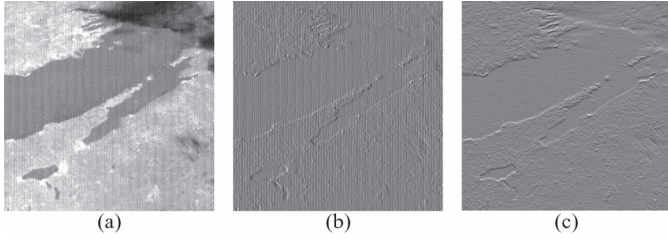


Fig. 1. (a) MODIS image band 21 with stripes and random noise. (b) Horizontal derivative. (c) Vertical derivative.

Fig. 1, we show the unidirectional gradients of the degraded MODIS image band 21 in horizontal and vertical directions. As shown in Fig. 1(b) and (c), the vertical gradient across stripes is severely affected by stripes, whereas the gradient along stripes is not influenced at all. This observation motivates us to constrain the gradient across stripes while preserving the gradient along stripes. To do this, we borrow the UTV from Bouali and Ladjal [9] that takes advantage of the directional signature of stripes. The UTV regularization is expressed as

$$R_{\text{UTV}}(\mathbf{u}) = \lambda_1 \|\nabla_x \mathbf{u}\|_1 + \lambda_2 \|\nabla_y(\mathbf{u} - \mathbf{f})\|_1. \quad (2)$$

Here,  $\nabla_x$  and  $\nabla_y$  are horizontal and vertical derivative operators, respectively. In this letter, we regard the direction across the stripe as the  $x$ -axis and the direction along the stripe as the  $y$ -axis.  $\lambda_1$  and  $\lambda_2$  are the regularization parameters.

### C. Sparse Representation for Denoising

Sparse representation has been an arguably powerful prior for image restoration, such as image denoising, deblurring, and super-resolution [14]. In this section, we briefly recall the basics of sparse representation in image denoising.

In the *Sparseland* model, images are often decomposed into small patches to better fit the sparse representation assumption [14]. For the sparse representation theory, the image patch  $\mathbf{u}_{ij}$  can be approximated to a sparse linear combination of the columns with respect to a dictionary  $\mathbf{D} \in \mathbf{R}^{n \times k}$  ( $n < k$ ), i.e.,  $\mathbf{u}_{ij} \approx \mathbf{D}\boldsymbol{\alpha}_{ij}$ , where  $\boldsymbol{\alpha}_{ij} \in \mathbf{R}^k$  is the sparse coefficient. Inequality  $n < k$  means the dictionary  $\mathbf{D}$  is redundant. Thus, one can recover a sparse approximation  $\hat{\boldsymbol{\alpha}}_{ij}$  for  $\mathbf{u}_{ij}$  by

$$\hat{\boldsymbol{\alpha}}_{ij} = \arg \min_{\boldsymbol{\alpha}_{ij}} \sum_{ij} \|\boldsymbol{\alpha}_{ij}\|_0 \quad \text{s.t.} \quad \|R_{ij}\mathbf{u} - \mathbf{D}\boldsymbol{\alpha}_{ij}\|_2^2 \leq \varepsilon \quad (3)$$

where  $\|\boldsymbol{\alpha}_{ij}\|_0$  stands for the number of the nonzero entries in  $\boldsymbol{\alpha}_{ij}$ , operator  $R_{ij}$  is a binary matrix that extracts a square patch of size from the location  $(i, j)$  in image  $\mathbf{u}$ , and  $\varepsilon$  is the bounded representation error.

The dictionary plays an important role in sparse representation. In this letter, the K-SVD algorithm [14] is used to learn a dictionary from the degraded images. An image  $\hat{\mathbf{Z}}$  approximating to the clear image  $\mathbf{u}$  can be reconstructed by merging all the constructed patches and averaging the overlapping regions between the adjacent patches

$$\hat{\mathbf{Z}} = \left( \sum_{ij} R_{ij}^T R_{ij} \right)^{-1} \left( \sum_{ij} R_{ij}^T \mathbf{D} \hat{\boldsymbol{\alpha}}_{ij} \right). \quad (4)$$

Thus, the sparse representation-based regularization for denoising can be described as

$$R_{\text{SLD}}(\mathbf{u}) = \frac{\lambda_3}{2} \|\mathbf{u} - \hat{\mathbf{Z}}\|_2^2. \quad (5)$$

### D. Joint Destriping and Denoising Model

In this letter, we present a unified model to simultaneously remove the stripes and random noise by combining UTV- and SLD-based regularizations. Formally, given the striped and noisy image  $\mathbf{f}$ , the clear image  $\mathbf{u}$  is expected to be estimated

$$\hat{\mathbf{u}} = \arg \min_{\mathbf{u}} E(\mathbf{u}) \quad (6)$$

where

$$\begin{aligned} E(\mathbf{u}) &= \frac{1}{2} \|\mathbf{u} - \mathbf{f}\|_2^2 + R_{\text{UTV}}(\mathbf{u}) + R_{\text{SLD}}(\mathbf{u}) \\ &= \frac{1}{2} \|\mathbf{u} - \mathbf{f}\|_2^2 + (\lambda_1 \|\nabla_x \mathbf{u}\|_1 + \lambda_2 \|\nabla_y(\mathbf{u} - \mathbf{f})\|_1) \\ &\quad + \frac{\lambda_3}{2} \|\mathbf{u} - \hat{\mathbf{Z}}\|_2^2. \end{aligned} \quad (7)$$

We explain each term of the model in detail as follows.

- 1) The first term is the reconstruction constraint, i.e., the recovered image should be consistent with the observation with respect to the estimated degradation model.
- 2) The second term penalizes the  $\ell_1$ -norm of gradient across the stripe line to suppress the stripes. In other words, it favors a solution  $\mathbf{u}$  that its derivative along the  $x$ -axis is smooth.
- 3) The third term enforces the  $\ell_1$ -norm constraint on the difference between the gradient along the stripe of the desired and striped images, aiming to preserve gradient along the stripe.
- 4) The fourth term means that the recovered image can be well approximated by the training set. Because the random noise is random distributed, they will not be sparsely represented. Therefore, the random noise can be well suppressed.

The basic idea of the unified model is to penalize the gradients across the stripes of the restored image while preserving the gradients along the stripes of the restored image as the degraded image; meanwhile, the restored image should have a sparse representation in terms of the training images.

### E. Split Bregman Optimization

The proposed model (7) involves nonsmooth and nonseparable  $\ell_1$ -norm terms and is hard to minimize directly. We adopt the split Bregman iteration [15] to solve the minimization problem. The main idea is to convert the unconstrained minimization problem on  $\mathbf{u}$  in (7) into a constrained one by introducing two auxiliary variables  $\mathbf{d}_x = \nabla_x \mathbf{u}$  and  $\mathbf{d}_y = \nabla_y(\mathbf{u} - \mathbf{f})$ . Thus, the minimization (7) is equivalent to the constrained problem

$$\begin{aligned} \min_{\mathbf{u}} \quad & \frac{1}{2} \|\mathbf{u} - \mathbf{f}\|_2^2 + \lambda_1 \|\mathbf{d}_x\|_1 + \lambda_2 \|\mathbf{d}_y\|_1 + \frac{\lambda_3}{2} \|\mathbf{u} - \hat{\mathbf{Z}}\|_2^2 \\ \text{s.t.} \quad & \mathbf{d}_x = \nabla_x \mathbf{u}, \quad \mathbf{d}_y = \nabla_y(\mathbf{u} - \mathbf{f}). \end{aligned} \quad (8)$$

Furthermore, problem (8) can be transformed into an unconstrained minimization with strictly enforcing the constraints by applying the Bregman iteration

$$\min_{\mathbf{u}, \mathbf{d}_x, \mathbf{d}_y} \frac{1}{2} \|\mathbf{u} - \mathbf{f}\|_2^2 + \lambda_1 \|\mathbf{d}_x\|_1 + \lambda_2 \|\mathbf{d}_y\|_1 + \frac{\lambda_3}{2} \|\mathbf{u} - \hat{\mathbf{Z}}\|_2^2 + \frac{\alpha}{2} \|\mathbf{d}_x - \nabla_x \mathbf{u} - \mathbf{b}_x\|_2^2 + \frac{\beta}{2} \|\mathbf{d}_y - \nabla_y (\mathbf{u} - \mathbf{f}) - \mathbf{b}_y\|_2^2 \quad (9)$$

where  $\alpha$  and  $\beta$  are the Bregman penalization parameters. We adopt the alternating minimization scheme to solve model (9), which converts the original problem into three simpler minimization subproblems.

- The  $\mathbf{u}$ -related subproblem is

$$\min_{\mathbf{u}} \frac{1}{2} \|\mathbf{u} - \mathbf{f}\|_2^2 + \frac{\lambda_3}{2} \|\mathbf{u} - \hat{\mathbf{Z}}^k\|_2^2 + \frac{\alpha}{2} \|\mathbf{d}_x^k - \nabla_x \mathbf{u} - \mathbf{b}_x^k\|_2^2 + \frac{\beta}{2} \|\mathbf{d}_y^k - \nabla_y (\mathbf{u} - \mathbf{f}) - \mathbf{b}_y^k\|_2^2. \quad (10)$$

Problem (10) can be solved by Gauss–Seidel iteration.

- The  $\mathbf{d}_x$ -related subproblem is

$$\min_{\mathbf{d}_x} \lambda_1 \|\mathbf{d}_x\|_1 + \frac{\alpha}{2} \|\mathbf{d}_x - \nabla_x \mathbf{u}^{k+1} - \mathbf{b}_x^k\|_2^2. \quad (11)$$

It can be solved by using a shrinkage operator as follows:

$$\mathbf{d}_x^{k+1} = \text{shrink} \left( \nabla_x \mathbf{u}^{k+1} + \mathbf{b}_x^k, \frac{\lambda_1}{\alpha} \right) \quad (12)$$

where

$$\text{shrink}(r, \xi) = \frac{r}{|r|} * \max(r - \xi, 0). \quad (13)$$

- Similarly,  $\mathbf{d}_y$  can be obtained as  $\mathbf{d}_x$  parallelly

$$\begin{cases} \mathbf{d}_x^{k+1} = \text{shrink} \left( \nabla_x \mathbf{u}^{k+1} + \mathbf{b}_x^k, \frac{\lambda_1}{\alpha} \right) \\ \mathbf{d}_y^{k+1} = \text{shrink} \left( \nabla_y (\mathbf{u}^{k+1} - \mathbf{f}) + \mathbf{b}_y^k, \frac{\lambda_2}{\beta} \right). \end{cases} \quad (14)$$

Then, we update the Bregman variables in the following way:

$$\begin{cases} \mathbf{b}_x^{k+1} = \mathbf{b}_x^k + (\nabla_x \mathbf{u}^{k+1} - \mathbf{d}_x^{k+1}) \\ \mathbf{b}_y^{k+1} = \mathbf{b}_y^k + (\nabla_y (\mathbf{u}^{k+1} - \mathbf{f}) - \mathbf{d}_y^{k+1}). \end{cases} \quad (15)$$

Finally, the sparse coefficients can be updated by

$$\hat{\alpha}_{ij}^{k+1} = \arg \min_{\alpha_{ij}} \mu_{ij} \|\alpha_{ij}\|_0 + \|R_{ij} \mathbf{u} - \mathbf{D} \alpha_{ij}\|_2^2. \quad (16)$$

The orthonormal matching pursuit [14] is used to solve (16). Then, the image  $\mathbf{Z}^{k+1}$  can be updated by (4).

### III. EXPERIMENTS AND DISCUSSION

In our tests, simulated and real images were used to verify the proposed method. All the test images were normalized between [0, 1]. Three destriping methods, the UTV [9], the variational stationary noise remover (VSNR) [8], and the WFAF [3] were compared. In addition, two denoising methods, the SLD [14] and spectral–spatial adaptive hyperspectral TV (SSAHTV) [10] were tested. For fair comparison, we also combined the denoising method (SLD) with the destriping methods (VSNR and UTV). For instance, SLD–VSNR means denoising by SLD was performed before destriping by VSNR.

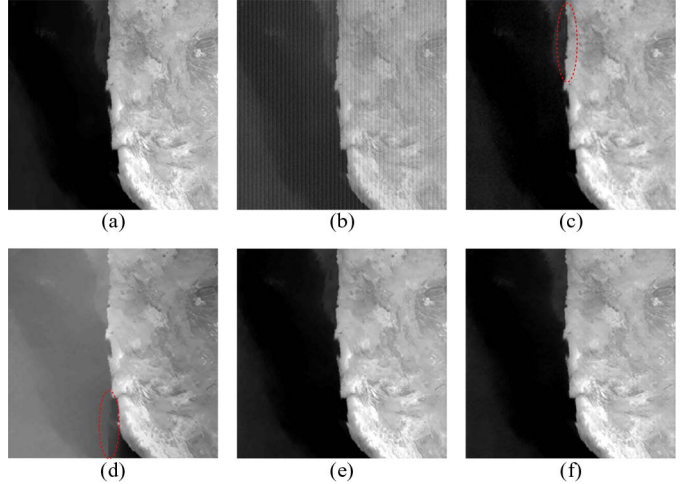


Fig. 2. Results in simulated Terra MODIS image band 31: (a) original band 31, (b) simulated degraded image, (c) WFAF, (d) SLD–UTV, (e) SLD–UTV + L2, and (f) ours.

In order to give an overall evaluation, several qualitative and quantitative indices were used. The qualitative indices include the visual performance and the mean cross-track profile. The quantitative indices include peak signal-to-noise ratio (PSNR), universal image quality index (UIQI) [18], noise reduction (NR) [9], Q-metric [19], and blind image quality index (BIQI) [20]. Note that PSNR and UIQI are full-reference indices, whereas NR, Q-metric, and BIQI are no-reference ones. NR is used to assess the destriping performance and Q-metric to assess the denoising performance. Small BIQI means good image quality. For the other indices, the larger value denotes the better restored images.

#### A. Simulated Experiment Results

In simulated experiments, we selected the image downloaded from [16], which was captured by Aqua MODIS on September 8, 2011 over the Africa. To illustrate the effectiveness of the proposed algorithm in removing stripes and random noise, we compare the results of different methods in Fig. 2. Fig. 2(a) shows a noise-free MODIS subimage of  $512 \times 512$  pixels. The degraded image [see Fig. 2(b)] was simulated by first adding stripes by two lines per ten lines and then the zero-mean white Gaussian noise with standard deviation  $\sigma = 10$ .

In Fig. 2 and its zoomed detailed regions in Fig. 3, it is shown that the proposed method gives the best destriping and denoising results, as compared with the results of other methods. In our result, on the one hand, the stripes and random noise are effectively removed, and on the other hand, the detail information is well preserved, with more convincing visual quality. For WFAF method, some residual random noise still remains, and some residual stripes still exit along the coast. In the SLD–UTV result, some structures with the same direction as stripes are corrupted together with the stripes, such as the coastline. Even worse, the intensities of the ocean region are evidently shifted. This is because the UTV approach lays too much emphasis on the smoothness of the images along a certain direction such that it tends to yield excessively destriped results. On the contrary, owing to the first fidelity term in our method,

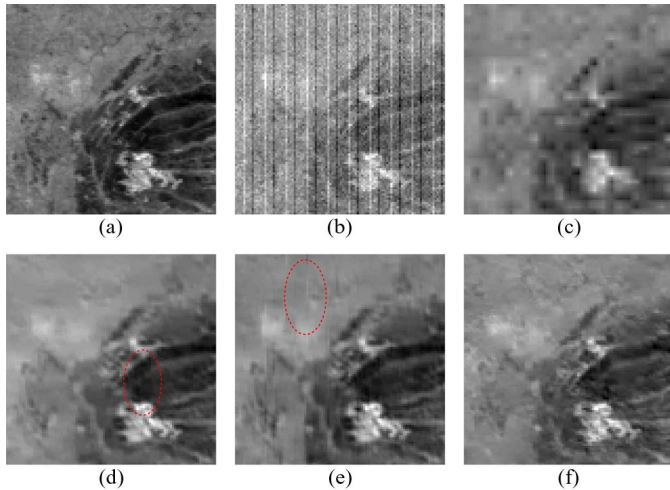


Fig. 3. Detailed regions cropped from Fig. 2.

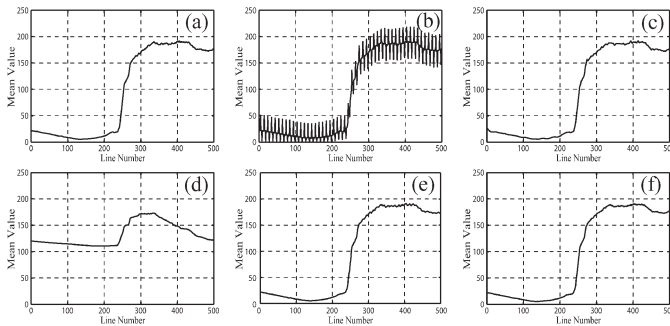


Fig. 4. Mean cross-track profiles of the images in Fig. 2.

TABLE I  
QUANTITATIVE ASSESSMENT OF THE SIMULATED  
MODIS IMAGE TERRA BAND 31

Index	Degraded	WFAF	SLD-UTV	SLD-UTV+L2	UTV+L2-SLD	Proposed
PSNR (dB)	23.67	32.06	10.55	32.57	29.62	<b>32.84</b>
UIQI	0.66	0.92	0.48	0.96	0.94	<b>0.96</b>

the image intensities are well preserved. We also compared the proposed method with the SLD (UTV + L2), where L2 represents the first term in the proposed model. As shown in Fig. 2(e), although most stripes are removed, there still exist some residual stripe fragments. The main reason is that the denoising process essentially damages the regular pattern of stripes, bringing the difficulty in subsequent destriping process.

Fig. 4 shows the mean cross-track profiles before and after processing. It can be observed that the mean cross-track profiles of the original and our result are mostly similar and quite smooth as expected. Table I lists the PSNR and UIQI values of the simulated test. It can be seen that the proposed method has obtained the best performance.

### B. Real Experimental Results

In addition, we test the effectiveness of the proposed algorithm on real data. In Fig. 5, we show the subimage and recovered results by different methods on Aqua MODIS image band 21. The image was captured on November 12, 2011, over the United States west coast (downloaded from [16]). The stripes and random noise are moderate, and the stripes

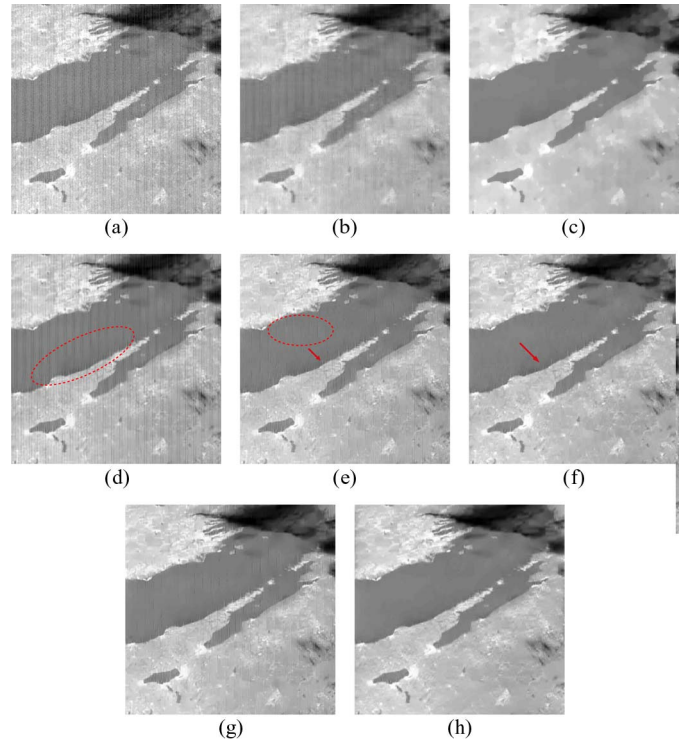


Fig. 5. Results in Aqua MODIS image band 21: (a) original image, (b) WFAF, (c) SSAHTV, (d) SLD, (e) SLD-VSNR, (f) SLD-UTV, (g) VSNR-SLD, and (h) ours.

TABLE II  
QUANTITATIVE ASSESSMENT OF THE REAL MODIS IMAGES

Image	Aqua band21		
	NR	Metric Q	BIQI
Degraded	--	19.01	57.29
WFAF	9.25	19.54	56.20
SSAHTV	11.62	22.95	45.46
SLD-VSNR	5.06	21.92	43.56
VSNR-SLD	5.46	22.24	40.47
SLD-UTV	5.97	22.36	40.16
Proposed	<b>12.02</b>	<b>23.72</b>	<b>37.82</b>

are periodic. The proposed method produces a more visually pleasing result, compared with the results of other methods. As indicated by the mark in Fig. 5(d), the SLD denoising process has damaged the regular pattern of stripes, leading to some broken fragments in stripe lines. As a result, the subsequent destriping results obtained by VSNR and UTV, in Fig. 5(e) and (f), exhibit residual stripes at the broken places. The residual stripes are also observed in Fig. 5(g) by VSNR-SLD. Indices NR, Q-metric, and BIQI, as listed in Table II, show that our method has achieved the best performance among the tested methods.

Moreover, the results on Hyperion hyperspectral image are given in Fig. 6. The image was captured by NASA's EO-1 Hyperion satellite on June 15, 2009, over Lake Monona (downloaded from [17]). This image contains severe nonperiodic stripes and some dead pixels near the right boundary. Visual inspection shows that our method outperforms the compared methods with respect to reducing noise, minimizing artifacts,

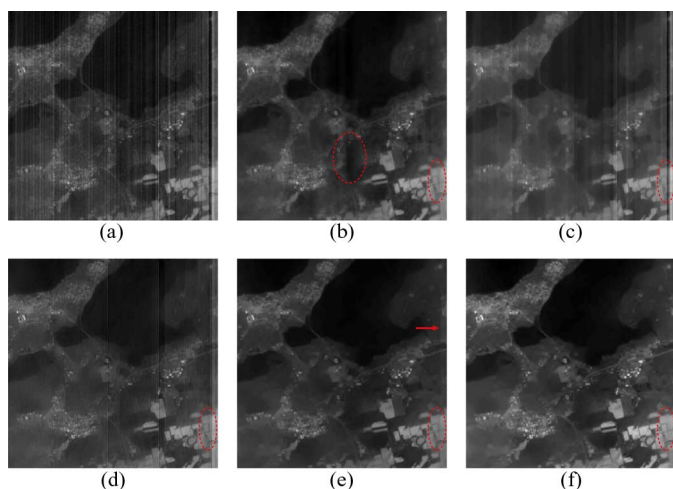


Fig. 6. Results in Hyperion image band 205: (a) original image, (b) WFAF, (c) SSAHTV, (d) SLD-VSNR, (e) SLD-UTV, and (f) ours.

and preserving detail information. More interestingly, our method repairs the dead pixels near perfectly.

#### IV. CONCLUSION

In this letter, we have proposed a simultaneous destriping and denoising method by combining the UTV and SLD. The proposed method can remove stripes and random noise simultaneously, as well as preserve the structure and detail information, whereas many existing techniques fail to achieve these. The qualitative and quantitative assessments demonstrate that the proposed method outperforms those methods that handle stripes and random noise separately. In the current model, the brute force search method for solving (16) containing the  $\ell_0$ -norm is time consuming. For an image of size  $256 \times 256$ , our method takes about 10 min in MATLAB 2010a on a personal computer with a 3.4-GHz CPU and 2-GB memory. In the future, we will incorporate the fast techniques [21] for the  $\ell_0$ -norm to speed up the algorithm.

#### ACKNOWLEDGMENT

The authors would like to thank Prof. A. Abd-Elrahman of the School of Forest Resources and Conservation, University of Florida, Gainesville, FL, USA, for kindly providing the wavelet Fourier adaptive filter code. They would also like to thank the handling editor and anonymous reviewers for their valuable remarks.

#### REFERENCES

- [1] Y. Chen, N. M. Nasrabadi, and T. D. Tran, "Hyperspectral image classification using dictionary-based sparse representation," *IEEE Trans. Geosci. Remote Sens.*, vol. 49, no. 10, pp. 3973–3985, Oct. 2011.
- [2] M. Joshi and A. Jalobeanu, "MAP estimation for multiresolution fusion in remotely sensed images using an IGMRF prior model," *IEEE Trans. Geosci. Remote Sens.*, vol. 48, no. 3, pp. 1245–1255, Mar. 2010.
- [3] R. Pande-Chhetri and A. Abd-Elrahman, "De-striping hyperspectral imagery using wavelet transform and adaptive frequency domain filtering," *ISPRS J. Photogramm. Remote Sens.*, vol. 66, no. 5, pp. 620–636, Sep. 2011.
- [4] J. S. Chen, Y. Shao, H. D. Guo, W. M. Wang, and B. Q. Zhu, "Destriping CMODIS data by power filtering," *IEEE Trans. Geosci. Remote Sens.*, vol. 41, no. 9, pp. 2119–2124, Sep. 2003.
- [5] F. L. Gadallah, F. Csillag, and E. J. M. Smith, "Destriping multisensor imagery with moment matching," *Int. J. Remote Sens.*, vol. 21, no. 12, pp. 2505–2511, Jan. 2000.
- [6] P. Rakwatin, W. Takeuchi, and Y. Yasuoka, "Stripe noise reduction in MODIS data by combining histogram matching with facet filter," *IEEE Trans. Geosci. Remote Sens.*, vol. 45, no. 6, pp. 1844–1856, Jun. 2007.
- [7] H. Shen and L. Zhang, "A MAP-based algorithm for destriping and inpainting of remotely sensed images," *IEEE Trans. Geosci. Remote Sens.*, vol. 47, no. 5, pp. 1492–1502, May 2009.
- [8] J. Fehrenbach, P. Weiss, and C. Lorenzo, "Variational algorithms to remove stationary noise: Applications to microscopy imaging," *IEEE Trans. Image Process.*, vol. 21, no. 10, pp. 4420–4430, Oct. 2012.
- [9] M. Bouali and S. Ladjal, "Toward optimal destriping of MODIS data using a unidirectional variational model," *IEEE Trans. Geosci. Remote Sens.*, vol. 49, no. 8, pp. 2924–2935, Aug. 2011.
- [10] Q. Yuan, L. Zhang, and H. Shen, "Hyperspectral image denoising employing a spectral-spatial adaptive total variation model," *IEEE Trans. Geosci. Remote Sens.*, vol. 50, no. 10, pp. 3660–3677, Oct. 2012.
- [11] H. Othman and S.-E. Qian, "Noise reduction of hyperspectral imagery using hybrid spatial-spectral derivative-domain wavelet shrinkage," *IEEE Trans. Geosci. Remote Sens.*, vol. 44, no. 2, pp. 397–408, Feb. 2006.
- [12] G. Y. Chen and S.-E. Qian, "Denoising of hyperspectral imagery using principal component analysis and wavelet shrinkage," *IEEE Trans. Geosci. Remote Sens.*, vol. 49, no. 3, pp. 973–980, Mar. 2011.
- [13] B. Rasti, J. R. Sveinsson, M. O. Ulfarsson, and J. B. Benediktsson, "Hyperspectral image denoising using 3D wavelets," in *Proc. IEEE IGARSS*, 2012, pp. 1349–1352.
- [14] M. Elad and M. Aharon, "Image denoising via sparse and redundant representations over learned dictionaries," *IEEE Trans. Image Process.*, vol. 15, no. 12, pp. 3736–3745, Dec. 2006.
- [15] T. Goldstein and S. Osher, "The split Bregman method for  $\ell_1$  regularized problems," *SIAM J. Imag. Sci.*, vol. 2, no. 2, pp. 323–343, May 2009.
- [16] <http://ladsweb.nascom.nasa.gov/>
- [17] <http://compression.jpl.nasa.gov/hyperspectral/imagdata/>
- [18] Z. Wang and A. C. Bovik, "A universal image quality index," *IEEE Signal Process. Lett.*, vol. 9, no. 3, pp. 81–84, Mar. 2002.
- [19] X. Zhu and P. Milanfar, "Automatic parameter selection for denoising algorithms using a no-reference measure of image content," *IEEE Trans. Image Process.*, vol. 19, no. 12, pp. 3116–3132, Dec. 2010.
- [20] A. K. Moorthy and A. C. Bovik, "A two-step framework for constructing blind image quality indices," *IEEE Signal Process. Lett.*, vol. 17, no. 5, pp. 513–516, May 2010.
- [21] J. S. Pan and Z. X. Su, "Fast  $\ell_0$ -regularized kernel estimation for robust motion deblurring," *IEEE Signal Process. Lett.*, vol. 20, no. 9, pp. 841–844, Sep. 2013.